J Mater Sci (2009) 44:5288–5296
DOI 10.1007/s10853-009-3666-6

FERROELECTRICS

Nanoscale defects and microwave properties of $(BaSr)TiO_3$ ferroelectric thin films

T. J. Jackson · I. P. Jones

Received: 17 March 2009 / Accepted: 4 June 2009 / Published online: 23 June 2009

Abstract Thin film ferroelectrics may have important applications in microwave devices but in general have significantly worse properties than bulk material. This is principally because of secondary and point defects. The natures of the defects are reviewed and strategies to study and remove them outlined.

Introduction

Tunable components operating in the microwave band (1–100 GHz) may be utilized in many types of communications, providing optimal use of available bandwidth, signal encoding and decoding and directionality under low power, voltage control. Application platforms range in scale from mobile phones to radar systems and in location from shipping to satellites. The sensitivity of the permittivity of ferroelectric materials to electric field bias makes them attractive in these applications. Thin films offer savings in size and weight compared with bulk materials. They also afford smaller capacitance values and lower tuning voltages. These details are discussed in [1], a key paper in that it was an early example of the compatibility between high temperature superconductors (HTS) and barium strontium titanate (BST). HTS gave a huge impetus to oxide film growth which led to increased activity in ferroelectrics [2–6]. Barium strontium titanate has become the material of choice for studies and development at ambient and low temperature as the variation in Curie temperature across the solid solution provides considerable flexibility [5]. Films are generally used in the paraelectric state to avoid domain wall losses and hysteresis. There are recent reviews of the state of the art in ferroelectric-superconductor devices [7] and room-temperature devices [8, 9].

It is generally true that the tunability and losses in thin film ferroelectrics are worse than those of bulk material. The objectives of this study are to survey the connections between microstructure and dielectric properties of BST films at microwave frequencies and to show and suggest how engineering at the nanoscale may be used to control the functional properties. We will draw on examples from the literature and from the work of our own research group.

For microwave devices, the range of substrates is limited [10]. Substrates must have low permittivity, low dielectric loss and temperature-independent dielectric properties. These considerations rule out $SrTiO_3$, a common substrate for high quality growth of perovskites. Substrates should be isotropic, which counts against sapphire, and ideally not twinned, which counts against lanthanum aluminate. Electrode layers must have high conductivity at microwave frequencies, which rules out oxide conductors such as $SrRuO_3$ and explains the initial enthusiasm for HTS. Thus for real microwave devices, the practical substrates are magnesium oxide and metallised silicon. Dysprosium and gadolinium scandates are good, but expensive. Given that epitaxy is likely to be compromised by the choice of substrate, strain and defect structure (nano-structure) are key topics in thin film development. Both are intimately connected to film growth mode.

The structure of this study is as follows. In the section "Dielectric properties of BST thin films at microwave

T. J. Jackson (✉)
School of Electronic, Electrical and Computer Engineering, University of Birmingham, Birmingham B15 2TT, UK
e-mail: T.J.Jackson@bham.ac.uk

I. P. Jones
School of Metallurgy and Materials, University of Birmingham, Birmingham B15 2TT, UK

frequencies" there is a broad survey of the dielectric properties of ferroelectric thin films at microwave frequencies. The section "The defect structure of BST and BST thin films" considers the defect structure of the (Ba, Sr)TiO_3 system in general and in thin films in particular. The section "Connections between defect structure and microwave properties" reviews the connections between defect structure and microwave properties and shows evidence that defect structure at the nanoscale is important. In the "Conclusions" there are suggestions for future research.

Dielectric properties of BST thin films at microwave frequencies

In analysis at microwave frequencies the relative permittivity should be expressed as a complex quantity $\varepsilon(E) = \varepsilon'(E)(1 - j\tan\delta(E))$: the real part $\varepsilon'(E)$is often referred to simply as the 'permittivity', $\tan\delta(E)$is the ratio of the imaginary and real parts of $\varepsilon(E)$ and E is the dc bias field. The rate of energy dissipation from the microwave signal into other forms ('dielectric loss') is given by

$$W(E) = \frac{\varepsilon_0 \varepsilon'(E) E_0^2}{2} \omega \tan\delta(E) \quad (1)$$

where E_0 is the amplitude of the microwave electric field, and ω is the angular frequency of the microwave signal. In Eq. 1 the field dependencies are included implicitly to show that, since both the permittivity and loss tangent of ferroelectrics are sensitive to bias field, the assessment of materials needs rather full characterization in order to be of value. Equation 1 also shows that the ideal microwave dielectric has a modest permittivity and a low loss tangent.

There are two common ways of defining tunability. The first is as the ratio of the real part of the permittivity in zero bias to that in dc field bias,

$$\eta = \frac{\varepsilon'(0)}{\varepsilon'(E)}. \quad (2)$$

The second is the relative tunability expressed as a percentage,

$$\eta_r = \frac{100(\varepsilon'(0) - \varepsilon'(E))}{\varepsilon'(0)}, \quad (3)$$

so $\eta = 100/(100 - \eta_r)$. A useful parameter for comparing films is the commutation quality factor or CQF [5]

$$\text{CQF} = \frac{(\eta - 1)^2}{\eta \tan\delta(0) \tan\delta(E)}. \quad (4)$$

The CQF is only meaningful when comparing ferroelectric materials if the electric field is specified, because η is a function of bias field. Furthermore, losses in the electrodes should be removed in the data analysis. The CQF is also implicitly a function of frequency. Although the intrinsic permittivity determined by the soft mode behaviour is a constant up to 100 GHz other processes related to structure or ferroelectric domains may introduce frequency dependencies [9, 11–15]. An additional complication is that conduction at the film–electrode interface may cause a frequency-dependent dissipation [16].

The properties of bulk BST will depend a great deal on composition and form (ceramic or single crystal) so it is not possible to give simple 'bulk' values for loss tangent, tunability and CQF. However, in general one may say that in the compositions which are paraelectric at room temperature and considered useful or microwave devices ($0.25 \leq x \leq 0.7$) values of the permittivity and loss tangent in zero field are in the range 1,000–5,000 and 0.001–0.02 at room temperature. The peak values of permittivity are of the order of 10^4, far higher than ever observed in thin films at microwave frequencies. Finally, CQF values are reported in the range 10^3–10^4 [5, 8, 9, 17].

Thin film ferroelectrics may be incorporated into device and test structures in one of two general configurations, as shown in Fig. 1. In the co-planar geometry, Fig. 1a, the

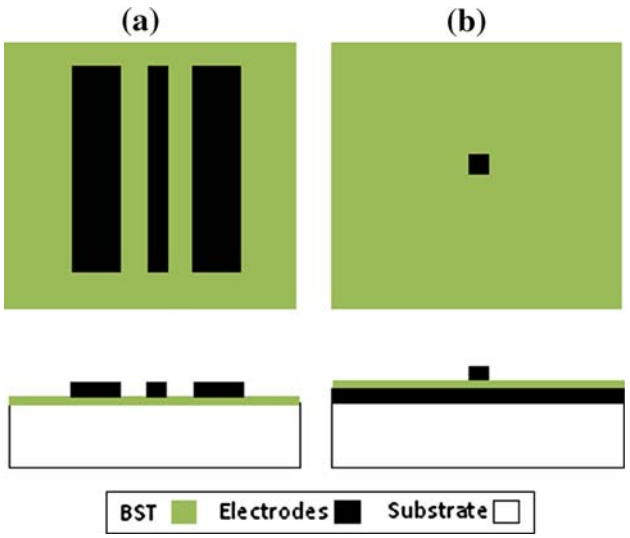

Fig. 1 Cross sectional and side views of co-planar (**a**) and parallel plate (**b**) geometries for thin film microwave devices [9, 18]. A co-planar geometry with a lower electrode (combination of **b** and **a**) may also be used. In **a** the outer two electrodes are ground planes and the inner, *narrower line* is the signal line. The bias is applied between the signal line and the ground planes. The electrodes are typically a micron thick. The signal line may be 5–50 μm in width, the ground electrodes are typically 200 μm or more in width. The lengths of the electrodes depend on the device design—they may be square or rectangular, up to several mm long and may be straight or meandering. In **b** the overlap of the top and bottom electrodes forms the varactor. The electric field associated with the microwave signal and the dc bias is applied between the two electrodes. The lower electrode is the ground plane. Typically the top electrode is a few microns square. The bottom electrode may also be patterned

film is deposited directly on top of an insulating substrate and then metallic or superconducting electrode layers are deposited and patterned on top of that. The structure shown is a ground-signal-ground co-planar waveguide or transmission line. Three-fingered microwave probes are used to make contact to both ground lines and to the signal line. The reflection and transmission coefficients (which are complex quantities) are measured with an instrument known as a vector network analyser. From these, the impedance and propagation constant of the transmission line can be calculated. These can be calculated to an accuracy of a few percent. Rather large error bars (perhaps as much as 10%) apply to the subsequent calculations of the permittivity of the film, which requires modelling of the fields in the structure and knowledge of the film thickness. The details, variations on the method and structure and some original references are assessed and reviewed in [18] and an error analysis presented in [19]. In the co-planar structure, the dc bias is applied between the signal and ground lines. These are typically 10–30 μm apart whereas the film is only 0.5 μm thick. The electric field within the ferroelectric film is quite uniform and parallel to the substrate plane. The 'filling factor', or fraction of field energy stored in the film is quite small: a substantial amount of field energy is stored in the air above the structure and the substrate below it and the 'effective permittivity' of the film/air/substrate may be as low as 20 even though the film itself has a permittivity of 1,000. Taking an electrode thickness of 0.5 μm and length of 1 mm with a 25 μm gap between signal and ground lines a quick estimate of the capacitance is 2 fF. Bias voltages of the order of 100 V between the ground and signal lines produce fields of the order of 4 V μm^{-1}.

The capacitance and bias field are higher in the second test geometry, the parallel plate structure of Fig. 1b. In this structure, the top electrode could be perhaps 5 μm^2 and this defines a 'parallel-plate' capacitor with a conducting bottom electrode. Since the film thickness is one tenth of the side of the capacitor, to a first approximation fringing fields can be ignored. Furthermore, the variation in permittivity away from the edges of the top electrode also makes only a small correction to the capacitance, as can be seen from [20]. A typical capacitance in this case is of the order of 0.5 pF and tunability is also much higher for a given voltage, 100 V producing a field of 200 V μm^{-1}. To make measurements on the parallel plate structure, a single probe can be used to make contact to the top and bottom electrodes [21]. The measurement now is of the reflection coefficient of the structure. The top electrode has to be small: pads of areas approaching 1 mm^2 such as might be used in low frequency measurements would present a very large capacitance at microwave frequencies and thus a very small reactance: the test structure would be almost indistinguishable from a short circuit in the reflection measurement. This would create a large uncertainty in the measured permittivity. The parallel-plate device is short compared to the wavelength which means that equivalent circuit models rather than transmission line models can be used in the data analysis [22, 23].

In both measurement geometries, calibration procedures to remove parasitic inductance, capacitance and loss are essential to reliable measurements.

Films grown on oxide or metallic surfaces will grow differently, so it is difficult to use the two structures to compare dielectric properties parallel and perpendicular to the film plane. The microstructure of ferroelectric films on common substrates such as MgO and Pt/Si is often columnar, the columns arising from growth on different terraces on the substrate surface and/or the meeting of slightly misoriented growth fronts [24–26]. Such columnar films tend to have relaxed the misfit strain. Modelling of the dielectric properties to include columnar boundaries and interfacial layers of different properties from the film bulk can provide insight into the most desirable microstructure [22]. In this study, though, attention is concentrated on smaller scale structure at the nanoscale, the defect structure.

An indicative collection of dielectric data on thin film BST measured at microwave frequencies is presented in Table 1. The data cover a 15-year period from 1993 to 2008. In device engineering the CQF of a device is often specified in terms of the device voltage, capacitance is given rather than permittivity and the loss tangent of the whole device, including electrode losses, is important. In assembling Table 1, only references from which the CQF can be specified in terms of electric field and which remove the contribution of the electrodes to the measured loss tangent are used. This is so that the ferroelectric materials can be compared directly. For microwave applications, a CQF of at least 2,000 is desirable [5]. For a commonly attained tunability of 1.5 (see Table 1) this requires an average loss tangent of 0.009, which few groups have attained in thin films. It is known that at the thickness (of the order of 100 nm) required for microwave devices, the differences between the properties of films and bulk materials are not simply due to a size effect: measurements on sliced crystals of similar and smaller thickness show bulk properties [27].

Referring to Table 1 the first clear feature is the higher bias field available for the films grown on metals, where the parallel plate geometry is possible. However, in these cases, the BST is not as tunable as in the best films on oxide substrates. The influence of epitaxy and growth mode appears to be strong. In most references where the permittivity-bias curves are shown, the real part of the permittivity is already approaching a minimal value in the

Table 1 Examples of zero bias dielectric properties and commutation quality factor reported for BST films at specified frequency f and temperature *T*

Material	f (GHz)	T (K)	ε (0)	tanδ (0)	η	CQF	E (V μm^{-1})	Reference
$SrTiO_3$ on $LaAlO_3$	11	4	920	0.05	1.7	463[a]	8	[3]
$Ba_{0.5}Sr_{0.5}TiO_3$ on MgO	1–20	300	770	0.067	1.5	85	6.7	[28]
$Ba_{0.5}Sr_{0.5}TiO_3$ on $LaAlO_3$	1–20	300	2545	0.167	2.2	71	6.7	[28]
$Ba_{0.03}Sr_{0.97}TiO_3$ on MgO	4	15	430	0.019	1.2	187	1.2	[29]
$Ba_{0.3}Sr_{0.7}TiO_3$ on Al_2O_3	1	300	NA	0.012	2	16000	40	[30]
$Ba_{0.25}Sr_{0.75}TiO_3$ on Pt(Au)/Si	20	300	164	0.01	1.7	5228	7	[22]
$SrTiO_3$ on MgO as grown	8	78	900	.0051	1.50	7600	10	[31]
$SrTiO_3$ on MgO annealled	8	78	600	.0038	1.25	3209	10	[31]
$Ba_{0.5}Sr_{0.5}TiO_3$ on MgO	20	300	900	0.005	1.2	600	1.6	[32]
$Ba_{0.5}Sr_{0.5}TiO_3$ on MgO	20	300	1800	0.055	2.0	275	3.2	[33]
$SrTiO_3$ on $DyScO_3$	10	300	3500	0.05	2.6	98	5	[35]
$Ba_{0.25}Sr_{0.75}TiO_3$ on Pt/Si	2	300	728	0.022	1.4	208	32.5	Unpublished
$Ba_{0.5}Sr_{0.5}TiO_3$ on $LaAlO_3$	1	300	1429	0.0098	1.74	420	6	[36]
$Ba_{0.25}Sr_{0.75}TiO_3$ on $LaAlO_3$	1	300	715	0.0047	1.42	331	6	[36]
$Ba_{0.5}Sr_{0.5}TiO_3$ on Pt/Si	1	300	368	0.0168	1.43	501	30	[36]
$Ba_{0.25}Sr_{0.75}TiO_3$ on Pt/Si	1	300	208	0.0155	1.27	281	30	[36]
BST90/10:BST75/25:BST60/40 on Pt/Si	0.5	300	291	0.0125	1.34	5521	150	[37]
BST90/10:BST75/25:BST60/40 on Pt/Si	10	300	261	0.0763	1.27	12	150	[37]
Mg-doped BST90/10:BST75/25:BST60/40 on Pt/Si	0.5	300	201	0.005	1.17	988	150	[37]
Mg-doped BST90/10:BST75/25:BST60/40 on Pt/Si	10	300	189	0.040	1.14	11	150	[37]

Only material specific data is chosen i.e. electrode losses are negligible or have been removed from in the analysis

[a] The bias dependence of the loss tangent is not given, so the CQF has been estimated from the zero bias loss tangent alone. The loss tangent normally decreases with bias so the actual CQF may be higher

available bias field, which implies that the five-fold reduction in permittivity attainable in bulk material [5, 8] is not available in thin films. The loss tangents are also generally much higher than in bulk. The upshot is that few groups achieve CQF values comparable with bulk material.

There is a reasonable correlation between low loss tangent and low zero field permittivity. It is stronger for the films on oxide substrates, Fig. 2a, than on metal electrodes, Fig. 2b. This correlation is a general characteristic of dielectric relaxation processes [38]. There is a very strong linear correlation between tunability and zero field permittivity. This is shown explicitly in Fig. 2c and d. Thus, there is also a link between low tunability and low loss tangent. However, the loss tangents are, in almost all cases, much higher than in bulk material and the permittivity and tunability are lower than in bulk material. This suggests extrinsic causes of the values of these parameters and that lower loss and higher tunability should be available.

Equation 4 shows a stronger influence of loss tangent on the CQF than the tunability. Figure 2e and f bear this out: indeed for films on metal bottom electrodes (Fig. 2f) there is almost no correlation between CQF and tunability. Thus, tunability can be sacrificed in pursuit of the lowest loss tangents. This motivated the choice of the low Curie temperature, 25% Ba composition for devices at room temperature [22] which achieved very promising CQF values of the order of 10^3. However, as stated above, both the tunability and loss tangent seem to have extrinsic origins.

Achievement of high CQF requires concentration on both increasing tunability and reducing loss tangent, with particular emphasis on the latter, in order to reduce the extrinsic contributions to their values. The section "Connections between defect structure and microwave properties" presents evidence that a high density of threading dislocations is correlated with low tunability and that the high loss tangents are connected with point defects.

Before going further, another extrinsic influence on tunability which has been discussed in the literature should be mentioned. There can be space charge or depletion layers beneath the surface of the ferroelectric [39–41]. In this case, tuning may occur due to the change in width of the depletion layer as a function of bias field, as in a semiconductor varactor. This mechanism may be significant if the width of the depletion layer is less than the separation of the electrodes [6, 42–44]. The situation is therefore particularly likely to arise if the oxygen stoichiometry of the films is not close to being correct, because

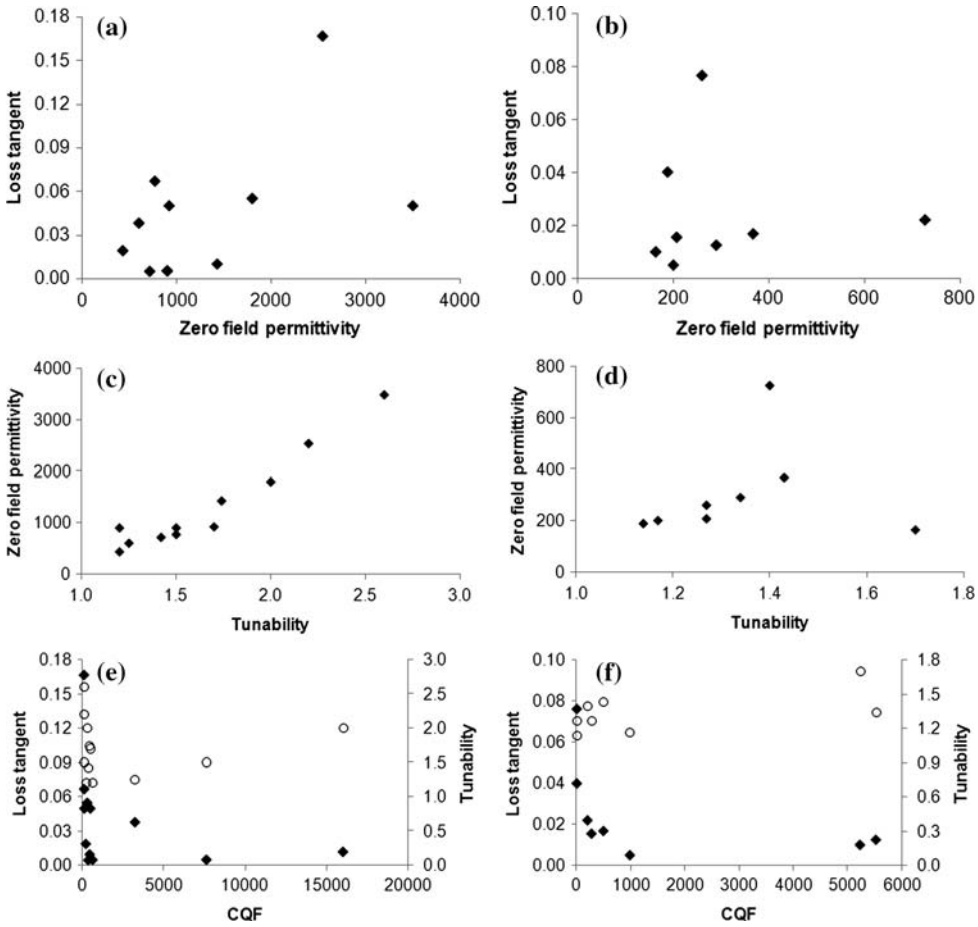

Fig. 2 Correlations between **a** loss tangent and real part of permittivity for films grown on oxide surfaces, **b** loss tangent and real part of permittivity for films grown on metal bottom electrodes, **c** permittivity and tunability for films grown on oxide surfaces, **d** permittivity and tunability for films grown on metal bottom electrodes, **e** loss tangent (◆) and tunability (○) and CQF for films grown on oxide surfaces, **f** loss tangent (◆) and tunability (○) and CQF for films grown on metal bottom electrodes

then the point defect and free charge density can be high [45, 46]. Since free charges are involved, such tuning may be accompanied by a large loss tangent [6]. If the tuning were indeed due to depletion layer effects, then Raman spectra of the lattice modes would be insensitive to the same bias which produces tunability. This insensitivity has been observed [47]. In other measurements of lattice modes in other films, however, a clear correlation between dielectric tuning and mode hardening was seen [48].

The defect structure of BST and BST thin films

Secondary defects (dislocations)

From the literature on dislocations in strontium and barium titanate bulk and films it is known that dislocations with Burgers vectors of both ⟨110⟩ type and ⟨100⟩ type are common. It is also known that ⟨110⟩ type dislocations tend to dissociate into partial dislocations and glide on the {110} planes [49–52]. The obvious difference between bulk and thin film STO and BST is the density of defects—obvious in the case of dislocations, but inferred in the case of point defects.

In an ideal world, a thin film would be grown on a substrate with which it has a low surface tension, a small lattice misfit and strong binding. In that case, layer-by-layer growth with a coherent film–substrate interface occurs and the small misfit between film and substrate is taken up by a uniform elastic strain in the film. As the film thickens dislocations may be nucleated at either the substrate–film interface or at the film surface and these dislocations accommodate the misfit strain [53, 54].

If the dislocations are nucleated at the substrate–film interface, this will most probably be at the edges of islands (where they exist) or at ledges on the substrate surface, both being stress concentrators. Those dislocations whose Burgers vectors relieve misfit strain will be favoured. If the Burgers vector lies in the interface, so will the resulting dislocation loop. The perfectly relieving edge dislocations with Burgers vectors lying in the interface can only form via this route.

If the dislocations originate at the film surface and then move down through the film, those with misfit strain-relieving Burgers vectors will be attracted to the substrate surface: the others will be repelled and remain as half loops hanging from the top surface. Each dislocation which successfully reaches the interface will leave two ‘threading’

dislocations at either end connecting the substrate–film interface with the top surface.

Dislocations may also originate in the substrate, in which case, depending on their Burgers vector, they may either lie in the substrate–film interface or form threading dislocations up to the surface of the film.

Studies of dislocations in thin films are consistent with these considerations. For example, in $Ba_{0.5}Sr_{0.5}TiO_3$ thin films grown epitaxially on (001) MgO substrates [55], it was found that many of the misfit dislocations were not of pure edge, [100] or [010] type. Instead, dislocations with Burgers vectors of the type $1/2\langle 101\rangle$ were present. The [001] component, perpendicular to the film substrate interface, is not able to relieve misfit strain, and so the misfit dislocations were found in a higher density than would have been expected for pure edge-type dislocations. In fact, the observed density was not sufficient to relax the misfit strain entirely, although the films were found to be totally relaxed. The '$\frac{1}{2}$'either reflects the film (via dissociation) or the substrate (e.g. via a ledge). The identification of the Burgers vectors of the threading dislocations using diffraction contrast is illustrated in Fig. 3. In this method, the crystal is tilted to satisfy the Bragg condition for a sequence of reflecting planes; when the displacement field of the dislocation (mostly parallel to b) lies in the diffracting planes (i.e. $g \cdot b = 0$) the image of the dislocation disappears. Most of the threading dislocations had b =$\langle 101\rangle$, twice that of the misfit dislocations. The method of formation of these was probably that described by Matthews [54]: glide of half loops from the film surface down to the film–substrate interface producing a misfit dislocation segment and two threading dislocations.

Primary (point) defects

These can be of thermal or constitutional origin. Thermal defects are of Schottky or Frenkel type. As regards constitutional defects, excess Sr may be incorporated by

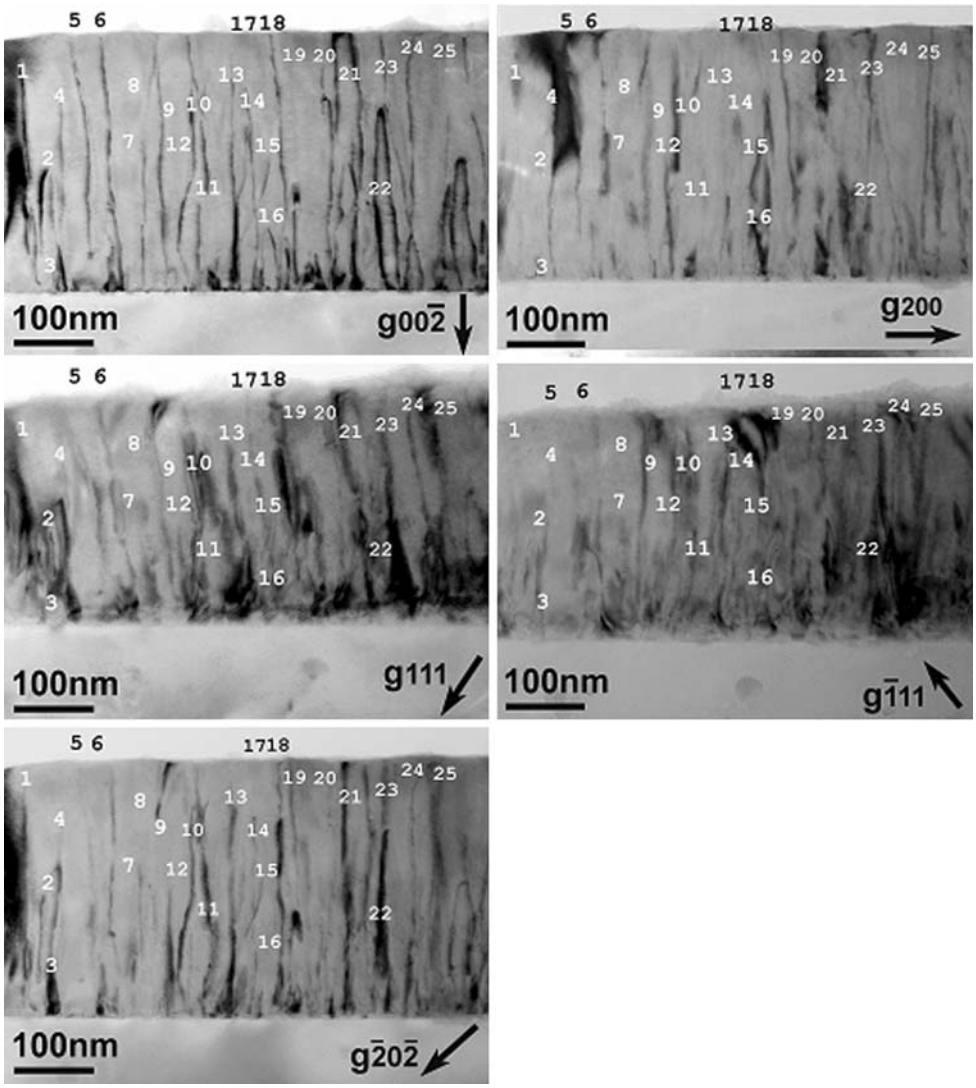

Fig. 3 Bright field TEM images of threading dislocations in an as-grown $Ba_{0.5}Sr_{0.5}TiO_3$ film [52]. The diffracted beam directions (g) are shown. The film has grown with cube-on-cube epitaxy with respect to the single crystal substrate: $\langle 100\rangle_{BST}//\langle 100\rangle_{MgO}$

Ruddleson-Popper phases: extra layers of SrO. However, excess Ti is not accommodated similarly. It may be accompanied by the formation of strontium vacancies and oxygen vacancies [56, 57], TiO_x phases [58, 59] and crystallographic shear structures [59]. Conventional methods of studying film composition such as energy dispersive X-ray analysis have an accuracy of the order of a few percent which is not really sufficient to address these issues. In very special circumstances, TEM can yield some information. However, the application of other techniques, such as precise lattice parameter measurements by X-ray diffraction, Rutherford backscattering spectroscopy and positron annihilation spectroscopy are urgently required.

Connections between defect structure and microwave properties

Secondary defects (dislocations)

In the early stages of growth, when the misfit strain is homogeneous throughout the thin film, there will be a resulting shift in the Curie temperature of the ferroelectric which may be predicted by the Landau–Ginzburg–Devonshire theory [60]. Ferroelectric phases forbidden in single crystals may be introduced [61]. In essence, though, tensile strain favours a ferroelectric polarization along the direction of strain and, through Poisson's ratio, leads to a reduction of the out-of-plane lattice parameter. This has been observed in BST on MgO substrates [62]. Furthermore, the ferroelectric phase should develop with in-plane polarization. We have used Raman spectroscopy to show this is the case for $Ba_{0.5}Sr_{0.5}TiO_3$ films on MgO [47]. Conversely, a compressive strain will favour expansion of lattice parameters perpendicular to the plane of the film, as has been shown to be the case for $Ba_{0.6}Sr_{0.4}TiO_3$ films on LSAT substrates [63]. At a particular measurement temperature, the dielectric properties will be similarly 'shifted' [35, 62, 64, 65]. Indeed, ferroelectricity at room temperature has been observed in $SrTiO_3$ thin films grown on $DyScO_3$ substrates [35, 66].

The primary influence of extended defects on dielectric properties is also through strain, but at the nanoscale. When dislocations are introduced as the film thickens, the small widespread homogeneous strain concentrates into local but heavily strained volumes around the misfit and threading dislocations. Transitions are smeared out by the inhomogeneous strain [34, 67]. For example, calculations have been performed of the strain field around misfit dislocations in epitaxial (001) $PbTiO_3$ films on (001) $LaAlO_3$ substrates, based on Landau–Ginzburg–Devonshire theory [68]. Here the misfit strain is compressive (around 3% at room temperature). The bulk Curie temperature of $PbTiO_3$ is 763 K [69] and the bulk spontaneous polarization is 0.75 C m^{-2} [70]. The analysis shows that the polarization may be enhanced by as much as one-third at a distance of several nanometres above an edge-type misfit dislocation. It may be suppressed by a similar amount between such dislocations in the periodic array along the film–substrate interface. Thus, an interfacial layer with quite different dielectric properties from the bulk of the film is inevitable. Such strain fields may also pin 90° twin walls [71]. In this context, it is interesting to note that a high density of dislocations has been observed beneath the surfaces of cut $SrTiO_3$ crystals [72]. The overlapping strain fields of these were correlated with a high-temperature ferroelectric phase suggested by X-ray diffraction as being present only near the surface of a crystal [73].

Misfit dislocations will only affect a thin layer of the film next to the substrate. Threading dislocations can affect the whole film and are probably more important in their effect on electrical properties. Indeed, several authors [33, 55, 63] have shown that reducing the density of threading dislocations in BST films by post-growth annealing increases the tunability significantly. For example, in the MgO/BST system described in the previous section, Tse and co-workers [33, 55] showed that ex-situ annealing of the grown thin film resulted in a 40% decrease in threading dislocation density and a concurrent 40% improvement in tunability. In addition, the breadth in temperature of the phase transition from the ferroelectric to the paraelectric state was very much reduced by the post-growth anneal. The annealing eliminated the dislocations with Burgers vectors with screw components, i.e. parallel to [001]; the density of edge and mixed type dislocations remained unchanged. Such results are strongly supportive of an association between the strain fields around the dislocations and inferior dielectric properties through the mechanisms discussed above. (The effect of the annealing on the point defect population could not be determined). A 'clean', uniform microstructure appears to be desirable. A smaller increase in loss tangent accompanied the increase in tunability, so the CQF was improved. It was still rather low though ($\approx 10^2$), because the loss tangent was still an order of magnitude larger than in the bulk.

The possibilities for engineering of growth modes and hence of defect structures have been shown recently, for strontium titanate grown on MgO [74]. Normally, as discussed above, in this epitaxial system with a 7.9% misfit, the strontium titanate grows in an island mode. We have used pulsed laser deposition to grow the strontium titanate. Films grown using laser pulses fired at a steady repetition rate of 5 Hz were found to be fully relaxed, with misfit dislocations and threading dislocations. The misfit dislocations were found to be dissociated as discussed above, with Burgers vectors $1/2[\bar{1}01]_{STO}$. These dislocations with

a screw component relieved only 2/3rds of the misfit strain. Other films were grown with bursts of pulses in the 'interval deposition' method [75]. In this method, the pulse repetition rate within the burst was in the range 60–100 Hz. The number of pulses within a burst was calibrated to be the number required to deposit one unit cell, in this case of the order of 20. A pause of 30 s duration was maintained between bursts. Such films grew under tension in-plane, i.e. unrelaxed, with a much lower density of threading dislocations than films grown in the standard way [74]. These results indicate that manipulation of growth kinetics may hold the key to the production of 'designer materials'. Indeed, homoepitaxial films grown under such conditions were almost indistinguishable from the substrate in cross-sectional TEM analysis. It may be concluded that the defects in the films grown on MgO were created in response to the misfit but that the kinetics of film growth limited the nucleation of those defects. The advantages of a rapidly pulsed deposition technique for growth manipulation compared with a steady deposition process are clear.

Point defects

The effect of an individual point defect is probably very small but the density of them may be very high [57, 76]. The approaches to line defects above may improve the tunability but there remains the general problem of the loss tangent being high compared with bulk material. Scott et al. [77] have argued that all non-intrinsic losses at microwave frequencies in $SrTiO_3$ films may be ascribed to hopping of oxygen vacancies and thus associated with point defects rather than line defects. Several authors have used comparisons of measured bias and frequency dependencies of the complex permittivity to deduce the important of charged defects in loss mechanisms, including dielectric loss and leakage currents [8, 17, 22, 30, 33, 34, 45, 47, 78] and oxygen vacancies are often associated with these defects. Oxygen stoichiometry is also known to be affected by strain [22, 79] as well, necessarily, as cation stoichiometry [80]. Indeed, cation stoichiometry has been shown to have a strong influence over dielectric losses in thin films [81]. Divalent dopants such as Mg^{2+} that sit on the Ti^{4+} site can compensate for oxygen vacancies and reduce dielectric loss [37].

Conclusions

The dielectric properties of BST thin films at microwave frequencies are strongly dependent upon the defect structure, at the nano-scale by line defects and at the atomic scale by point defects, although the balance between the effects of these is presently unknown. Further studies of control of the growth mode and of the resulting line defect structure via growth kinetics, and the effects on the dielectric properties at microwave frequencies, will be valuable. More careful control of film stoichiometry might well lead to a reduction in the wide scatter of dielectric properties shown in Table 1 as point defect density is better controlled.

The production of films with optimal microstructure for optimal properties is an opportunity for engineering realised down at the genuine nanoscale. This is 'Engineering' in the full meaning of the word—specification of desired properties, design to meet that specification and then implementation of the design followed by evaluation and modification. The experience gained in applying modern theoretical and experimental capabilities in analysis and deposition to ferroelectric thin films will transfer directly to studies and applications of ferromagnetic, magnetoelectric and multiferroic thin films

Acknowledgements We would like to acknowledge the Engineering and Physical Sciences Research Council for financial support. We would like to thank our colleagues P Bao, C Bayer, H Bouyanfif, R Chakalov, CNW Darlington, J Hriljac, WF Hu, F Huang, Y Koutsonas, MJ Lancaster, YH Liu, SRC McMitchell, JH Park, G Passeriuex, A Porch, HT Su, PM Suherman, RI Tchakalova, YY Tse and X Wang for their work and support.

References

1. Jackson CM, Kobayashi JH, Lee A, Pettiette-Hall C, Burch JF, Hu R, Hilton R, McDade J (1992) Microw Opt Technol Lett 5(72):2
2. Carroll KR, Pond JM, Chrisey DB, Horwitz JS, Leuchtner RE, Grabowski KS (1993) Appl Phys Lett 62:1845
3. Galt D, Price JC, Beall JA, Ono RH (1993) Appl Phys Lett 63:3078
4. Hermann AM, Yandrofski RM, Scott JF, Naziripour A, Galt D, Price JC, Cuchario J, Ahrenkiel RK (1994) J Supercond 7:463
5. Vendik OG, Hollman EK, Kozyrev AB, Prudan AM (1999) J Supercond 12:325
6. Miranda FA, Mueller CH, Cubbage CD, Bhasin KB, Singh RK, Harkness SD (1995) IEEE Trans Appl Supercond 5:3191
7. Scott JF (2007) In: Bussmann-Holder A, Keller H (eds) High T_c superconductors and related transition metal oxides. Springer-Verlag, Berlin
8. Tagantsev AK, Sherman VO, Astafiev KF, Ventkatesh J, Setter N (2003) J Electroceramics 11:5
9. Bao P, Jackson TJ, Wang X, Lancaster MJ (2008) J Phys D 41:063001
10. Hollmann EK, Vendik OG, Zaitsev AG, Melekh BT (1994) Sci Technol 7:609
11. Poplavko YM, Tsykalov VG, Molchanov VI (1969) Sov Phys Solid State 10:2708
12. Baniecki JD, Laibowitz RB, Shaw TM, Duncombe PR, Neumayer DA, Kotecki DE, Shen H, Ma QY (1998) Appl Phys Lett 72:498
13. Gevorgian S, Petrov PK, Ivanov Z, Wikborg E (2001) Phys Lett 79:1861
14. Booth JC, Takeuchi I, Chang KS (2005) Appl Phys Lett 87:082908

15. Tsurumi T, Li J, Hoshina T, Kakemoto K, Nakada M, Akedo J (2007) Appl Phys Lett 91:182905
16. Pervez NK, Park J, Lu J, Stemmer S, York RA (2005) Integr Ferroelectr 77:87
17. Vendik OG, Ter-Martirosyan LT (2000) J Appl Phys 87:1435
18. Suherman PM, Jackson TJ, Lancaster MJ (2007) Theory Tech 55:397
19. Petrov PK, Alford NMcN, Gevorgyan S (2005) Meas Sci Technol 16:583
20. Cheng LC, Lancaster MJ (2007) IET Microw Antennas Propag 1:453
21. Ma ZX, Becker AJ, Polakos P, Huggins H, Pastalan J, Wu H, Watts K, Wong YH, Mankiewich P (1998) IEEE Trans Electron Devices 45:1811
22. Vorobiev A, Rundqvist P, Khamchane K, Gevorgian S (2004) J Appl Phys 96(464):2
23. Sheng S, Wang P, Zhang XY, Ong CK (2009) J Phys D 42:015501
24. Chen CL, Shen J, Chen SY, Lao GP, Chu CW, Miranda FA, Van Kuels FW, Jiang JC, Meletis EI, Chang HY (2001) Appl Phys Lett 78:652
25. Park BH, Gim Y, Fan Y, Jia QX, Lu P (2000) Appl Phys Lett 77:2587
26. Koutsonas I, Hu WF, Jackson TJ, Jones IP, Lancaster MJ, Passerieux G, Chakalov RA, Chakalova RI, Darlington CNW (2004) Integr Ferroelectr 61(13):9
27. Chang LW, McMillen M, Morrison FD, Scott JF, Gregg JM (2008) Appl Phys Lett 93:132904
28. Chang W, Horwitz JS, Carter AC, Pond JM, Kirchoefer SW, Gilmore CM, Chrisey DB (1999) Appl Phys Lett 74:1033
29. Su HT, Lancaster MJ, Huang F, Wellhofer F (2000) Microw Opt Technol Lett 24:155
30. Razumov SV, Tumarkin AV, Gaidukov MM, Gagarin AG, Kozyrev AB, Vendik OG (2002) Appl Phys Lett 81:1675
31. Astafiev KF, Sherman VO, Tagantsev AK, Setter N, Kaydanova T, Ginley DS (2004) Appl Phys Lett 84:2385
32. Suherman PM, Jackson TJ, Koutsonas Y, Chakalov RA, Lancaster MJ (2004) IEEE MTT-S Int 1:265
33. Suherman PM, Jackson TJ, Tse YY, Jones IP, Chakalova RI, Lancaster MJ, Porch A (2006) J Appl Phys 99:104101
34. Suherman PM, Jackson TJ, Tse YY, Lancaster MJ (2006) Ferroelectrics 335:69
35. Chang W, Kirchoefer SW, Belloti JA, Qadri SB, Pond JM, Haeni JM, Schlom DG (2005) J Appl Phys 98:024107
36. Zhang SW, Wang P, Sheng S, Feng X, Ong CK (2008) J Appl Phys 104:124110
37. Cole MW, Weiss CV, Ngo E, Hirsch S, Coryell LA, Alpay SP (2008) Appl Phys Lett 92:182906
38. Frohlich H (1990) Theory of dielectrics dielectric constant and dielectric loss. Oxford University Press, Oxford
39. Chynoweth AG (1956) Phys Rev 102:705
40. Slack JR, Burfoot JC (1971) J Phys C Solid State Phys 4:898
41. Fitzgerald W, Darlington CNW (1976) Acta Crystallogr A 32:671
42. van der Berg RA, Blom PWM, Cillessen JFM, Wolf RM (1995) Appl Phys Lett 66:697
43. Matsuura H (2000) New J Phys 2:8.1
44. Bayer C, Jackson TJ (2006) Appl Phys Lett 89:022908
45. Hwang CS, Lee BT, Kang CS, Kim JW, Lee KH, Cho HJ, Horii H, Kim WD, Lee SI, Roh YB, Lee MY (1998) J Appl Phys 83:3703
46. Scott JF (1999) Ferroelectrics 232:905–914
47. Bouyanfif H, Suherman PM, Jackson TJ, Marssi MEI, Hriljac J (2008) J Appl Phys 103:114101
48. Sirenko AA, Bernhard C, Goinik A, Clark AM, Hao J, Si W, Xi XX (2000) Nature 404:373
49. Matsunaga T, Saka H (2000) Philos Mag Lett 80:597
50. Suzuki T, Nishi Y, Fujimoto M (1999) Philos Mag A 79:2461
51. Gao HJ, Chen CL, Rafferty B, Pennycook SJ, Luo GP, Chu CW (1999) Appl Phys Lett 75:2542
52. Chen JH, Lia CL, Urban K, Chen CL (2002) Appl Phys Lett 81:1291
53. Matthews JW, Blakeslee AE (1974) J Cryst Growth 27:118
54. Matthews JW (1975) J Vac Sci Technol A 12:126
55. Tse YY, Suherman PM, Jackson TJ, Jones IP (2008) Philos Mag 88:2505
56. Ohnishi T, Lippmaa M, Yamamoto T, Meguro S, Koinuma H (2005) Appl Phys Lett 87:241919
57. McGuire S, Keeble DJ, Mason R, Coleman PG, Koutsonas Y, Jackson TJ (2006) J Appl Phys 100:044109
58. Tse YY, Koutsonas Y, Jackson TJ, Passerieux G, Jones IP (2006) Thin Solid Films 515:1788
59. Suzuki T, Nishi Y, Fujimoto M (2000) Philos Mag A 80:621
60. Devonshire AF (1954) Adv Phys 3:85
61. Pertsev NA, Zembilgotoov AG, Tagantsev AK (1998) Phys Rev Lett 80:1988
62. Li H, Roytburd AL, Alpay SP, Tran TD, Salamanca-Riba L, Ramesh R (2001) Appl Phys Lett 78:2354
63. Canedy CL, Li H, Alpay SP, Salamanca-Riba L, Roytburd AL, Ramesh R (2000) Appl Phys Lett 77:1695
64. Chang W, Gilmore CM, Kim WJ, Pond JM, Kirchoefer SW, Qadri SB, Chrisey DB, Horwitz JS (2000) J Appl Phys 87:3044
65. Ban ZG, Alpay SP (2002) J Appl Phys 91:9288
66. Haeni JH, Irvin P, Chang W, Uecker R, Reiche P, Li YL, Choudhury S, Tian W, Hawley ME, Craigo B, Tagantsev AK, Pan XQ, Streiffer SK, Chen LQ, Kirchoefer SW, Levy J, Schlom DG (2004) Nature 430:758
67. Catalan G, Noheda B, McAneney J, Sinnamon I, Gregg JM (2005) Phys Rev B 72:020102(R)
68. Alpay SP, Misirliogu IB, Nagarajan V, Ramesh R (2004) Appl Phys Lett 85:2044
69. Jona F, Shirane G (1993) Ferroelectric crystals. Dover, Oxford
70. Lines ME, Glass AM (2001) Principles and applications of ferroelectrics and related materials. Clarendon Press, Oxford
71. Chu MW, Szafraniak I, Hesse D, Alexe M, Gösele U (2005) Phys Rev B 72:174112
72. Wang R, Zhu Y, Shapiro SM (1998) Phys Rev Lett 80:2370
73. Darlington CNW, O'Connor DA (1976) J Phys C Solid State Phys 9:3561
74. Tse YY, McMitchell SRC, Jackson TJ, Liu YH, Jones IP (2008) Ferroelectrics 368:287
75. Blank DHA, Koster G, Rijnders GAJHM, Van Setten E, Slycke P, Rogalla H (2000) J Cryst Growth 211:98
76. Mackie RA, Singh S, Laverock J, Dugdale SB, Keeble DJ (2009) Phys Rev B 79:014102
77. Scott JF, Galt D, Price JC, Beall JA, Ono RH, Dearaujo CAP, Mcmillan LD (1995) Integr Ferroelectr 6:189
78. Vendik OG, Platonova LM (1971) Sov Phys Solid State 13:1353
79. Petrov PK, Alford NMcN (2005) Appl Phys Lett 87:222902
80. Chan NH, Sharma RK, Smyth DM (1981) J Electrochem Soc 128:1762
81. Pervez NK, Hansen PJ, York RA (2004) Appl Phys Lett 85:4451